

Chiroptical response in coupled plasmonic nanostructures

Author: Redouan Boukafri Itahriouan

Facultat de Física, Universitat de Barcelona, Diagonal 645, 08028 Barcelona, Spain.

Advisor: Amílcar Labarta Rodríguez & Javier Rodríguez Álvarez

Abstract: This study delves into the chiroptical response in plasmonic twisted stacks of Au nanostructures with different rotational symmetries. Hybridization of the individual modes excited on each of the stack elements as a function of the twist angle induces a strong chiroptical response under circularly polarized light. The results show that the symmetry of the individual elements affects the charge distribution, modulating the magnitude and spectral position of the hybridized modes. Moreover, multipolar excitations more complex than the ideal in-phase and anti-phase expected hybridizations are found, causing a rich chiroptical response that can be easily adjusted by the twist angle. These systems may be applied as active platforms for detection of molecular chirality or for light polarization.

Keywords: Electromagnetism, Light-metal interactions, Coupled oscillators, Nanomaterials.

SDGs: This work is related to the SDGs 7.a and 9.5.

I. INTRODUCTION

Plasmonics studies how conduction electrons in metallic nanostructures interact with electromagnetic waves, particularly in the optical frequency spectrum [1]. This interaction gives rise to charge oscillation modes known as plasmons. This work focuses on Localized Surface Plasmon Resonances (LSPR), a non-propagating excitation that occurs when an electromagnetic wave with wavelength λ interacts with the electrons of a metal nanostructure at the interface with a surrounding dielectric medium.

The excitation of LSPR is associated with the generation of electromagnetic fields which depend on the shape, size, chemical composition, and surrounding medium of the nanostructures [2]. The interaction between the light and the nanostructures can be measured in terms of the absorption A and scattering S cross-sections (CS), whose sum constitutes the extinction CS, $E = S + A$. While A and S are virtual optical responses, extinction represents the probability that radiation interacts with a single metallic nanostructure through a plasmonic resonance and is directly measurable via light transmission.

Since LSPR arises from the coupling of the electron charge oscillations and an oscillating electromagnetic field, the resulting spectral profile is symmetrical in energy. As a result, the dependencies of A and S on the energy follow Lorentzian distributions:

$$L(\varepsilon) = \frac{1}{1 + \left(\frac{\varepsilon - \varepsilon_0}{\Gamma/2}\right)^2}, \quad (1)$$

where ε is the energy, ε_0 is the energy corresponding to the maximum amplitude of the resonance, and Γ is the full width at half maximum. Thus, the charge density distribution associated with LSPR can create a localized electric field near the interface, which becomes significantly intense given the proper conditions.

When the distance between two nanostructures is sufficiently small, the plasmon modes of the individual elements interact, leading to the formation of new hybridized modes with substantial field enhancement at LSPR compared to that of the isolated elements. These modes are identified as bonding and antibonding, depending on the relative phase difference in the excitation of the nanostructures. Bonding modes arise due to anti-phase coupling of plasmonic oscillations. The plasmon resonance shifts to longer λ compared to that of the uncoupled components due to attractive interactions. In contrast, anti-bonding modes arise from in-phase coupling of plasmonic oscillations between nanostructures. The energy of anti-bonding/bonding modes is higher/lower due to the effect of repulsive/attractive interactions. These hybridized modes are highly sensitive to the relative configuration of the interacting nanostructures, including their spacing and orientation.

Chirality, the property of being non-superimposable on a mirror image, is crucial in many natural and synthetic systems [3]. It is closely associated with circular dichroism, for which a chiral system exhibits different E under left-handed circularly polarized light (LCP) and right-handed circularly polarized light (RCP). This effect is quantified by the dissymmetry factor:

$$g = \frac{2(E_{LCP} - E_{RCP})}{E_{LCP} + E_{RCP}}, \quad (2)$$

where E_{LCP} and E_{RCP} are the extinction cross-sections under LCP and RCP illumination, respectively. While natural chiral materials typically display weak dichroism with values of g smaller than 10^{-3} [4], plasmonic nanostructures, with helicoidal or twisted configurations, can amplify this effect significantly [2]. This enhancement is a direct result of the near fields associated with LSPR that increases the interaction cross-sections among the different parts of the chiral nanostructure.

The aim of this work is to investigate the chiroptical response of twisted stacks constituted of two planar

Au nanostructures, examining how both the rotational symmetry of the individual elements and the twist angle affect the hybrid excitations and the resulting dichroism.

II. RESULTS AND DISCUSSION

In this work, the optical response of plasmonic Au nanostructures was studied using Lumerical's Finite-Difference Time-Domain (FDTD) software [5]. Through a discretization of space and time, this method solves Maxwell's equations using finite-difference numerical integration. Further details are provided in the Supplementary Material.

The dielectric constants of Au were obtained from Johnson and Christy [6]. The refractive index of the surrounding medium is 1.45 (SiO_2).

A. Isolated bar and tribar

Two Au plasmonic elements with different rotational symmetry are studied. On the one hand, bars with length \times width \times height of $165 \text{ nm} \times 50 \text{ nm} \times 40 \text{ nm}$ and having 2-fold symmetry. On the other hand, the so-called *tribars*, consisting of three bars with dimensions of $82.5 \text{ nm} \times 50 \text{ nm} \times 40 \text{ nm}$ emanating from a center along directions forming 120° between them and exhibiting 3-fold symmetry. Fig. 1 shows a top view of the two elements. Note that the volume swept by both structures when rotated around their centers is identical.

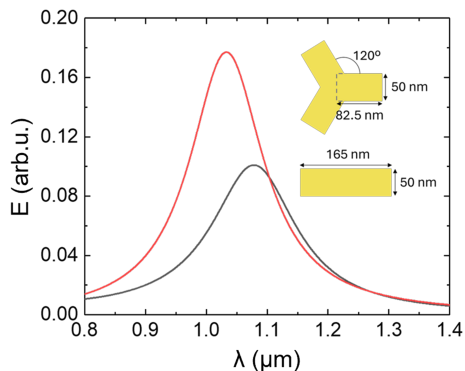


FIG. 1: Simulated E as a function of λ for both the bar (black curve) and the tribar (red curve) using a LCP source. A top view of the two elements indicating their dimensions is added as an inset.

The responses of an isolated bar and tribar were simulated under a LCP source within $800 \text{ nm} \leq \lambda \leq 1400 \text{ nm}$. In Fig. 1, the less energetic resonance peaks in E for the two nanostructures are shown. There is a blue shift for the tribar relative to the bar. This shift arises from the larger surface area of the tribar, which intensifies the near fields due to electrostatic polarization. Thus, plasmonic modes become more energetic, and E is enhanced by the interaction of the radiation with a larger metallic area.

B. Plasmon hybridization

To analyze the hybridization of the modes studied in section A, two bars were stacked on top of each other, separated by a variable gap size d , as shown in the inset to Fig. 2(b). Fig. 2(a) illustrates how the peak in E splits into two distinct ones due to plasmon coupling between the bars. In a first approximation, the high-energy, anti-bonding mode corresponds to the two bars polarized as in-phase dipoles along the longitudinal axes of the bars, while the low-energy, bonding mode corresponds to the bars acting as anti-phase dipoles.

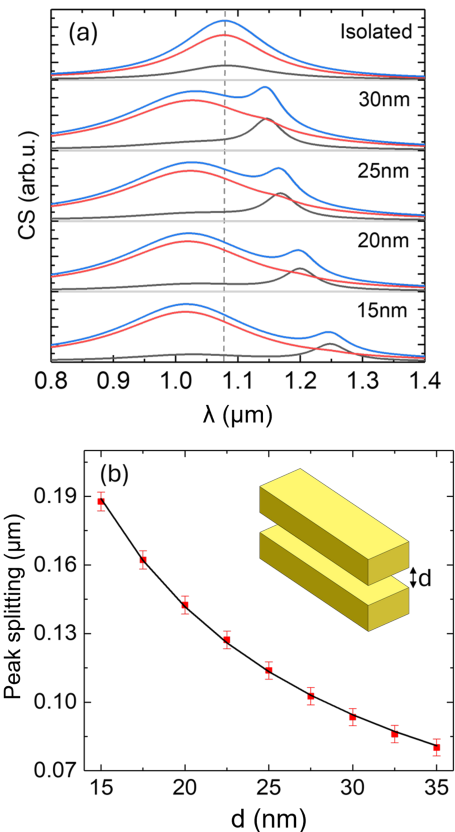


FIG. 2: (a) Simulated E (blue curve), S (red curve), and A (black curve) for an isolated bar and the stack, for different values of d . (b) Spectral splitting of the two E peaks as a function of d . The inset shows a scheme of the bar stack.

As the gap size decreases, one of the peaks shifts to shorter λ with respect to the isolated bar, while the other shifts to longer λ . For the anti-bonding mode, reducing the gap between in-phase dipoles increase charge repulsion, thereby raising the system's energy (blueshift). Conversely, for the bonding mode, reducing the gap between anti-phase dipoles enhances charge attraction, lowering the system's energy (redshift).

The total dipole moment of the system is related to S efficiency. For the anti-bonding peak, the net dipole moment is large, resulting in significant S and minimal A (bright mode). In contrast, for the bonding peak, the

dipole moment is small, resulting in low S and dominant A (dark mode).

Fig. 2(b) shows the splitting of the two hybridized modes as a function of d . Interestingly, this splitting is directly related to plasmon coupling between the nanostructures. Fitting Lorentzian profiles (Eq. (1)) to A (for further details see the Supplementary Material) reveals a $1/d$ decay. Thus, the splitting, to a first order of approximation, reflects an energy relationship governed by the Coulomb interaction between the two bars. In Fig. 2(a), although both peaks shift, the bonding mode exhibits the largest shift variation both in λ and ε .

C. Dichroism of the bar and tribar dimers

By stacking two bars (and two tribars) separated by $d = 15$ nm and rotating the upper nanostructure in a right-handed direction (from an upper view) to break the mirror symmetry, the structure becomes chiral. The schematic configurations are shown in the insets to Fig. 3(c) and 3(f). Fig. 3 shows colormaps for E as a function of the twist angle θ between the two elements for the bar (Fig. 3(a) and 3(b)) and the tribar dimers (Fig. 3(d) and 3(e)) under RCP and LCP illumination. The peak positions were determined by fitting Lorentzian profiles (Eq. (1)) to A and are also shown in Fig. 3 as dashed circles and squares. Once again, the position of the high-energy peak remains relatively constant, while the low-energy peak varies significantly as θ changes.

Due to the specific rotational symmetry of each of the

two monomers, the angle range is limited to 90° for the bars and 60° for the tribars. In both cases, the dimer chirality favors the excitation of the bonding mode for LCP, since the light rotates in the opposite direction to the chirality of the nanostructure. For RCP, the light excites the two monomers similarly due to the small phase delay of the light over d , favoring the anti-bonding mode. This occurs because the two monomers tend to have in-phase charge distributions, severely hampering the anti-phase resonance. At $\theta = 0^\circ$ and $\theta = 90^\circ$, the excitation of the two bars is identical for both light polarizations, as no chirality exists in these configurations. The same behavior occurs for the tribars at $\theta = 0^\circ$ and $\theta = 60^\circ$.

In Fig. 3, one observes that as θ increases, the coupling between the monomers weakens. This occurs because, in both bonding and anti-bonding modes, rotation causes an increase in the average distance between the charges on the facing sides of the two monomers. Thus, increasing θ yields a similar effect to increasing d .

In both dimers, a similar anti-crossing behavior of the two excitations occurs as a function of θ (see Fig. 3). The differences between the two spectra are due to two main factors. First, the larger area of tribars makes the plasmonic modes more energetic and E higher in intensity. Secondly, for tribar dimers, the peak splitting decreases significantly less with θ . This is because the range of θ in the tribar is smaller than in the bar (60° versus 90°). As a result, the increase in the average distance between charges in the facing monomers is smaller in the tribar as θ increases, leading to a smaller variation in the splitting.

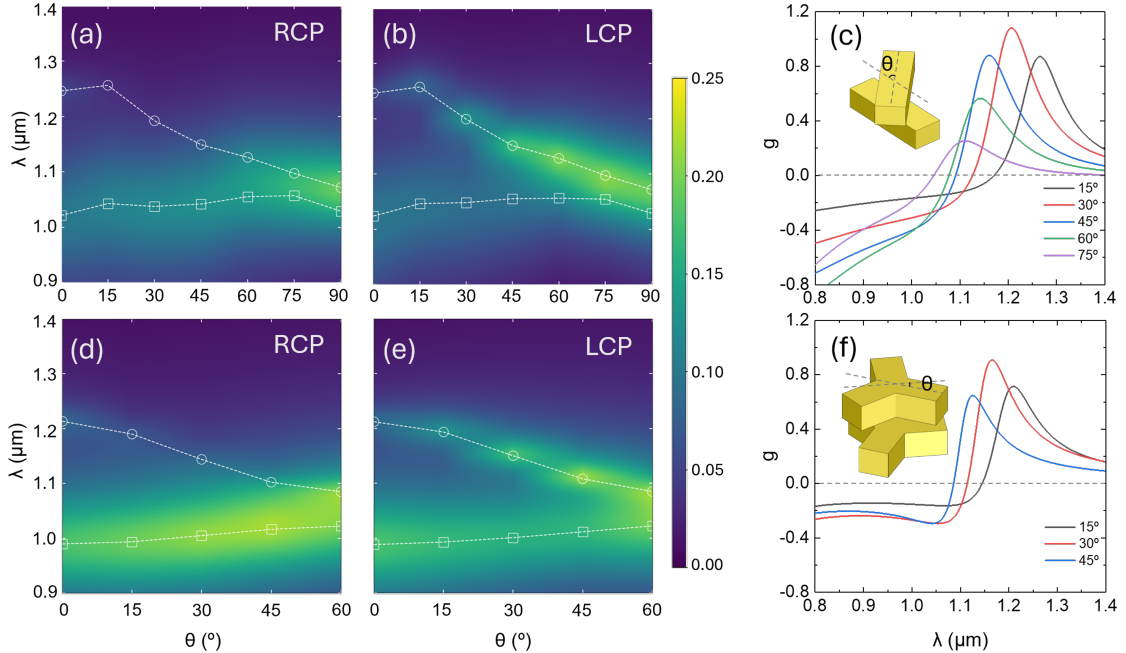


FIG. 3: Colormaps depicting E for the bar dimer (a, b) and the tribar dimer (d, e) for RCP and LCP, respectively. Empty circles and squares represent the spectral position of the two Lorentzian peaks fitted to the simulated data. Dashed lines are guidelines to the eye. Calculated values of g according to Eq. (2) for the dimer of twisted bars (c) and tribars (f) for different angles. Insets to (c) and (f) show schemes of the twisted bars and tribars, respectively.

The dichroism for the two systems is shown in Fig. 3(c) and 3(f). g values, calculated using Eq. (2), are significantly higher than those observed in most molecular systems [4]. In chiral molecules, dichroism arises from the helical motion of displacement currents induced by circularly polarized light [2], which causes the electron clouds to follow helical paths. In contrast, these dimers exhibit a more complex interaction by excitation of both displacement and real currents within the nanostructures. Unlike molecules, plasmonic structures generate much stronger real and displacement currents due to the large number of free electrons in metal nanoparticles. The strong plasmon coupling enhances the chiral flow of currents, particularly displacement currents between the nanostructures, increasing the chiroptical response [2].

As previously mentioned, in the bonding mode, the net dipoles of the two monomers are out of phase, resulting in intense displacement currents between them. Conversely, in the anti-bonding mode, the displacement currents, induced by the in-phase dipoles, are much weaker. Thus, large values of g are associated with the light-handedness selective excitation of the bonding mode as it happens in these dimers under LCP and RCP illumination (see colormaps in Fig. 3). Thus, maxima in g curves, shown in Fig. 3(c) and 3(f), shift to lower λ as θ increases, following the blue shifting of the bonding mode.

It is worth noting that, in both dimers, the maximum g (for the computed data) occurs around 30° . To explain this, it first should be considered that plasmon coupling is highest at $\theta = 0^\circ$, but the system is not chiral at this angle, resulting in $g = 0$. As the θ increases, the system becomes chiral, causing g to rise. This increase continues at the expense of the decrease in plasmon coupling until a compromise is reached between the two opposing tendencies around $\theta = 30^\circ$, where dichroism is optimized due to a large chiral effect of the structure on the incoming light and still enough plasmon coupling.

Finally, it is worth noting that in both types of dimers, similar values of g are obtained at the anti-bonding mode. However, at the bonding, the 2-fold symmetry results in a stronger chiral response.

D. Charge distribution

In Fig. 4, the charge distributions at the facing nanostructure interfaces are shown for an angle of $\theta = 0^\circ$ at the corresponding λ for both bonding and anti-bonding modes. Note that for the bar dimer (Fig. 4(a) and 4(b)), if one focuses on the charge near the bar ends, the modes are almost dipolar. In contrast, for the tribar (Fig. 4(c) and 4(d)), the 3-fold symmetry of the monomer disrupts the dipole excitation of each of the bars in the monomer. However, there is still an overall dipole excitation of the monomer, for which two ends consistently carry a higher charge than the third one. Thus, the net dipole polarization of the monomers is more efficient in the bar dimers than in the tribar ones due to geometric frustration.

In both dimers, a complex polarization appears in

the lower monomer for the anti-bonding mode. What happens is that, once the upper monomer is polarized, its plasmonic modes interact with those of the second monomer, giving rise to modes that are different from the ideal in-phase configuration shown in previous studies [2], [7]. In this case, the lower monomer partially compensates the polarization of the upper one, while attempting to get in phase. In contrast, the bonding mode behaves more following the anti-phase model. Here, the upper monomer positively influences the attempt of the second monomer to align in anti-phase.

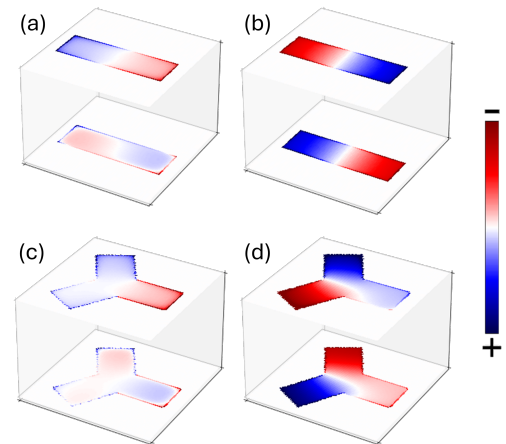


FIG. 4: Simulated charge distributions for the bar and tribar dimers under LCP light at $\theta = 0^\circ$: (a, c) anti-bonding modes and (b, d) bonding modes for the bar and tribar dimers, respectively.

The net dipole moments of each monomer in the bar and tribar dimers were calculated based on the induced charge distributions within the nanostructures, by summing the contributions from the charge in the mesh points. Then, their evolution under the influence of circularly polarized light was computed over a light cycle. In Fig. 5, the dipole moments of the two monomers in the bar dimer (Fig. 5(a) and 5(b)) and the tribar dimer (Fig. 5(c) and 5(d)) at $\theta = 45^\circ$ and $\theta = 30^\circ$, respectively, are shown for the anti-bonding and bonding modes. For the bar dimer, the trajectory of the dipoles resembles a highly eccentric ellipse. This behavior arises because the bars efficiently localize charges at their ends. An exception is observed in the lower bar in the anti-bonding mode. Similar to what is seen in Fig. 4, the lower bar is strongly influenced by the upper bar. As the peak splitting decreases with increasing θ , the anti-bonding mode adopts characteristics of the bonding one in terms of charge distribution. Eventually, both modes become indistinguishable. On the contrary, for the bonding mode, the angle between the semi-major axes of the ellipse tends to 45° as expected. Recall that the separation distance d induces a phase shift between the bars. In this mode, the system exhibits an anti-phase behavior, where the dipoles align in opposite directions while adapting to the geometry of the bars.

For the tribar dimer, the trajectories of the dipoles are nearly circular. This configuration allows the tribars to freely align their dipole moment with the incident light's electric field. Despite the complexity of the anti-bonding mode, in the case of $\theta = 30^\circ$, the energy splitting is sufficient to distinguish the in-phase mode, where the dipoles attempt to align in phase. In the bonding mode, the charges align well in an anti-phase configuration while still respecting the geometry of the monomers.

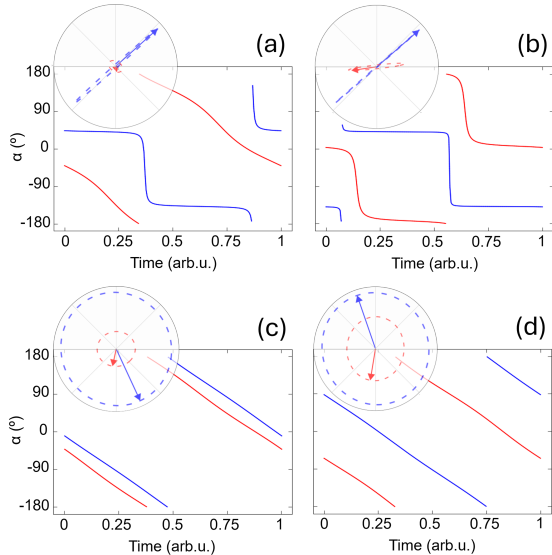


FIG. 5: Simulated evolution of α for the upper (blue curve) and lower (red curve) bars and tribars over time, normalized to a full rotation of the electric field under LCP light. (a) and (b) show α for the bonding and anti-bonding modes for the bar dimer at $\theta = 45^\circ$, while (c) and (d) show α for the bonding and anti-bonding modes for the tribar dimer at $\theta = 30^\circ$. Insets display the dipole moments for the upper (blue vector) and lower (red vector) nanostructures at an arbitrary time, with dashed curves showing their trajectories.

The main plots in Fig. 5 highlight the differences in the trajectories of the dipole moments over a light cycle arising from the two rotational symmetries of the monomers by displaying the angle α , determined by projecting the dipole moments onto the plane at the center of the interface between the monomers, and measuring the angle relative to an arbitrary axis. α is plotted as a function of time over a cycle, with 180° identified as -180° . The

2-fold symmetry tends to localize the moments along the long axes of the bars to minimize energy. Thus, the direction of the dipole angle is metastable, with an abrupt transition taking place when the moments invert their orientation. In contrast, the 3-fold symmetry introduces a third end that can polarize to varying degrees depending on the instantaneous orientation of the electric field of the incident light. This breaks the metastability and allows the system to keep the magnitude of the dipole moments nearly constant while adjusting their orientation to the incident electric field. As a result, the dipole moments rotate in a way that keeps the angle between the upper and lower moments approximately constant.

III. CONCLUSIONS

We studied the chiroptical response of stacks of two different monomers: bars and tribars. Using numerical simulations, we characterized the plasmon coupling between the monomers, proving its strong dependence on the gap size and twist angle between them, and the rotational symmetry of the monomers. Plasmon coupling results in dimers exhibiting a strong chiroptical response, with large values of g at the hybridized bonding mode.

The charge distribution shows that 2-fold symmetry tends to localize the charge at the ends of the bars, leading to minimal variation in the direction of the dipole moments of the monomers over a light cycle. In contrast, the 3-fold symmetry of the tribars adapts more efficiently to the rotation of the incident electric field, resulting in a circular motion of the dipole moments of the monomers. Moreover, the 3-fold symmetry causes the average distance between charges in the facing monomers to increase less than in the 2-fold case as θ increases, resulting in stronger plasmon coupling.

Finally, while the bonding mode in both dimers aligns with the ideal anti-phase behavior, the anti-bonding mode shows a more complex response, challenging the assumed perfect in-phase behavior of previous studies.

Acknowledgments

Thanks to my advisors, Amílcar Labarta and Javier Rodríguez for their guidance and assistance. Also, many thanks to my family and friends for the immense support.

-
- [1] Novotny, L., and Hecht, B., *Surface plasmons. In Principles of Nano-Optics* (Chapter 12). Cambridge University Press (2012).
- [2] Wu, A., Tanaka, Y. Y., and Shimura, T. *Giant chiroptical response of twisted metal nanorods due to strong plasmon coupling*. APL Photonics 6, 126104 (2021).
- [3] Wang, X., and Tang, Z. *Circular dichroism studies on plasmonic nanostructures*. Small 13(1), 1601115 (2016).
- [4] Tang, Y., and Cohen, A. E. *Enhanced Enantioselectivity*

- in Excitation of Chiral Molecules by Superchiral Light*. Science, Vol. 332, Issue 6027, pp. 333-336 (2011).
- [5] Lumerical Inc. – *Innovative Photonic Design Tools*. Available online: <https://www.lumerical.com/>.
- [6] Johnson, P. B., and Christy, R. W. *Optical constants of the noble metals*. Phys. Rev. B 6, 4370 (1972).
- [7] Bai, B., Svirko, Y., Turunen, J., and Vallius, T. *Optical activity in planar chiral metamaterials: Theoretical study*. Phys. Rev. A 76, 023811 (2007).

Chiroptical response in coupled plasmonic nanostructures

Author: Redouan Boukafri Itahriouan

Facultat de Física, Universitat de Barcelona, Diagonal 645, 08028 Barcelona, Spain.

Advisor: Amílcar Labarta Rodríguez & Javier Rodríguez Álvarez

Resum: Aquest estudi investiga la resposta quiro-òptica en apilaments plasmonics retorçats de nanoestructures d'or amb diferents simetries de rotació. La hibridació dels modes individuals excitats en cada element de l'apilament en funció de l'angle de torsió indueix una forta resposta quiro-òptica sota llum polaritzada circularment. Els resultats mostren que la simetria dels elements individuals afecta la distribució de càrrega, modulant la magnitud i la posició espectral dels modes hibridats. A més, s'observen excitacions multipolars més complexes que les hibridacions ideals en fase i anti-fase esperades, donant lloc a una alta resposta quiro-òptica que es pot ajustar fàcilment mitjançant l'angle de torsió. Aquests sistemes poden aplicar-se com a plataformes actives per a la detecció de la quiralitat molecular o per a la polarització de la llum.

Paraules clau: Electromagnetisme, Interacció llum-metall, Oscil·ladors acoblats, Nanomaterials.

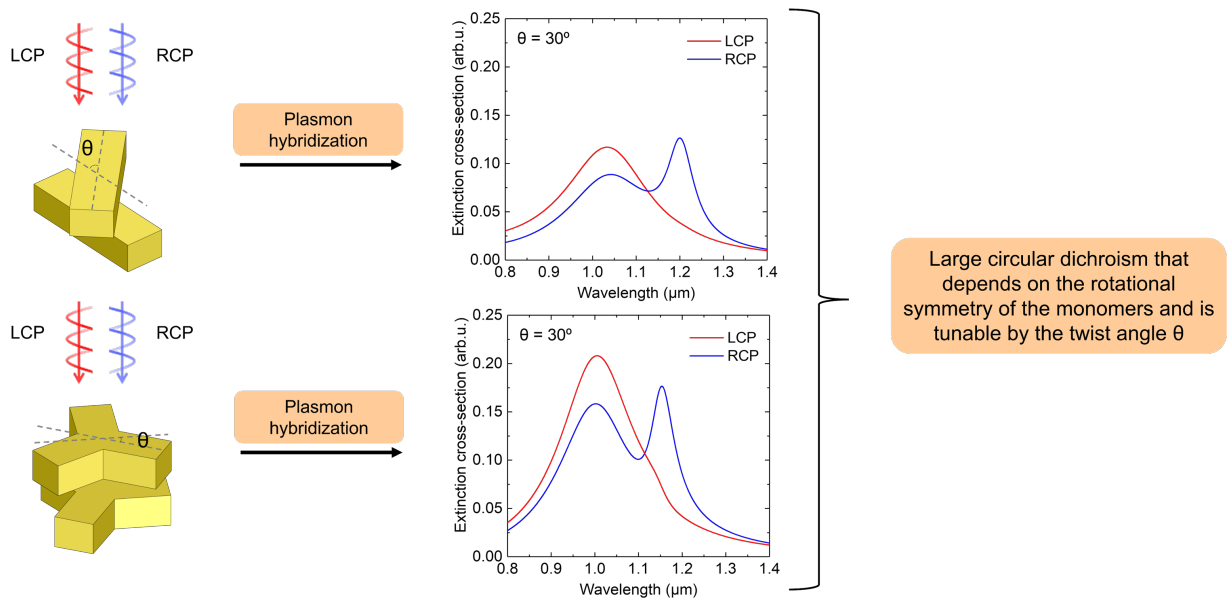
ODS: Aquest treball està relacionat amb els ODS 7.a i 9.5.

Objectius de Desenvolupament Sostenible (ODSs o SDGs)

1. Fi de la pobresa		10. Reducció de les desigualtats	
2. Fam zero		11. Ciutats i comunitats sostenibles	
3. Salut i benestar		12. Consum i producció responsables	
4. Educació de qualitat		13. Acció climàtica	
5. Igualtat de gènere		14. Vida submarina	
6. Aigua neta i sanejament		15. Vida terrestre	
7. Energia neta i sostenible	X	16. Pau, justícia i institucions sòlides	
8. Treball digne i creixement econòmic		17. Aliança pels objectius	
9. Indústria, innovació, infraestructures	X		

Per una banda, aquest treball contribueix a la innovació en el camp de la nanociència, investigant estructures plasmòniques amb propietats òptiques úniques. Aquesta línia de recerca és fonamental per a aplicacions industrials com sensors òptics, dispositius fotònics i tecnologia biomèdica avançada (Fita 9.5). Per altra banda, les propietats de ressonància plasmònica investigades en aquest estudi tenen potencial per millorar l'eficiència de les cèl·lules solars i altres dispositius d'energia renovable, optimitzant la captació i ús de la llum solar (Fita 7.a).

GRAPHICAL ABSTRACT



SUPPLEMENTARY MATERIAL

A. Lumerical FDTD software

Simulations were conducted using the FDTD method implemented in the commercial software Lumerical [5]. This method is based on the creation of a spatial and temporal mesh in order to solve Maxwell's equations on each point of the mesh. The software includes a visual interface which allows the creation of different simulations by customizing light sources and metallic structures with tabulated refractive indexes. Fig. S1 illustrates the stacked tribar configuration within the Lumerical interface.

Circularly polarized light sources were generated by combining two electromagnetic plane waves with a 90° phase difference. Multiple monitors were employed to measure quantities such as light intensity, the modulus of the electric field, the charge distribution, and A and S , with all results normalized to the incident amplitude.

To simulate the chiroptical response of the bar and tribar dimers as if isolated in space, the computational domain was enclosed by a lossy material known as a perfectly matched layer (PML), which absorbs incoming waves from all angles of incidence causing almost no reflections. After designing the system, simulations were carried out with a fixed time limit and a shutoff level of 10^{-11} . The shutoff indicator estimates the fraction of the remaining energy relative to the initial value and stops the simulation in case of divergence. If the shutoff level is not sufficiently low, the simulation results are influenced by cavity modes arising from the imperfect absorption of the PML.

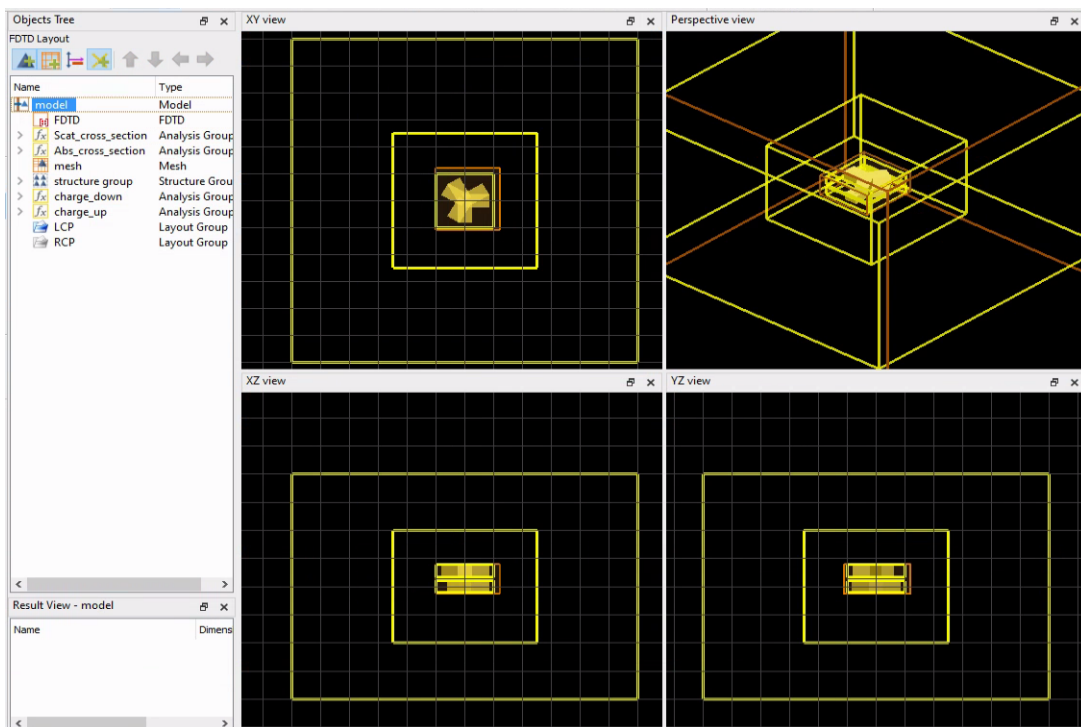


Fig. S1: Screenshot of Lumerical's visual interface simulating the chiroptical response of a tribar for $\theta = 30^\circ$ under a LCP source.

B. Lorentzian fits

To determine the positions of the centers of the two peaks in E , the Lorentzians in A were fitted using a nonlinear least-squares curve fitting method, employing the `curve_fit` function from the Python `scipy.optimize` library. The centers of the Lorentzian peaks in A and S are assumed to coincide, as the resonances occur at the same wavelength, a result confirmed after several simulations. Since S in the bonding mode does not produce a prominent peak, only the Lorentzians in A were fitted. Fig. S2 shows an example of the plot obtained from fitting the Lorentzians in A for a tribar stack with $\theta = 30^\circ$ under an LCP source. The fits are satisfactory, though a slight error is visible at the ends of the simulated curve. This is due to multipolar resonances at higher energies than those represented, which slightly affect the fits.

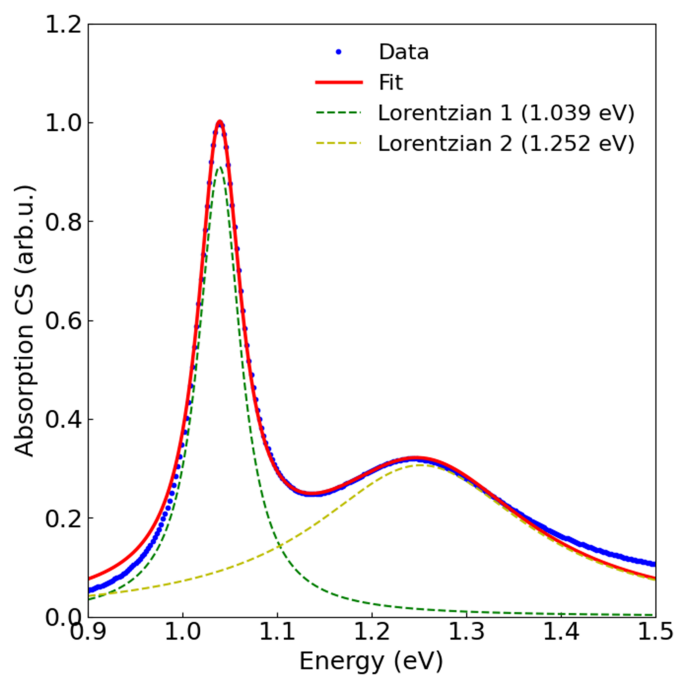


Fig. S2: Double Lorentzian fitting of the bonding and antibonding modes for the simulated A of a tribar stack with $\theta = 30^\circ$ under an LCP source. The values in parentheses show the center of each Lorentzian used in the fitting.